Unsupervised texture segmentation using a nonlinear energy optimization method

Sasan Mahmoodi
Newcastle University
School of Biology and Psychology
Psychology Division
Henry Wellcome Building, Framlington Place
Newcastle upon Tyne, NE2 4HH, United Kingdom
E-mail: Email: sasan.mahmoodi@ncl.ac.uk

Bayan S. Sharif
Newcastle University
School of Electrical, Electronic, and Computer Engineering
Merz Court
Newcastle upon Tyne, NE1 7RU, United Kingdom

Abstract. *A nonlinear functional is considered for segmentation of images containing structural textures. A structural texture pattern in an image is characterized by a certain amplitude spectrum, and segmentation of different patterns is obtained by detecting different regions with different amplitude spectra. A gradient-descent-based algorithm is proposed by deriving equations minimizing the functional. This algorithm, implementing the solutions minimizing the functional, is based on the level set method. An effective method employed in this algorithm is shown to be robust in a noisy environment. Experimental results demonstrate that the proposed method outperforms segmentation obtained by using the simulated annealing algorithm based on Gaussian Markov random fields. © 2006 SPIE and IS&T.* [DOI: 10.1117/1.2234370]

1 Introduction

Recently, variational methods in image and signal processing have attracted considerable attention. Segmentation using variational methods was initially introduced by Kass *et al.*[1] and was further developed as the geodesic active contours model and the level set method.[2] Texture segmentation using geodesic active contours in Ref. 3 is achieved by minimizing the length of the active contour in a Riemannian space (feature space), which is generated by applying the Gabor filters to the original textured image. Geodesic active contours were further developed as geodesic active regions by Paragios and Deriche[4] for supervised texture segmentation by considering the histograms of a set of Gabor filters applied on known textures. This scheme was further explored in Ref. 5 for unsupervised texture segmentation based on the frame theory.[3,2] Vese and Osher[6] also proposed a method based on the total variation suggested by Rudin *et al.*[7] for texture modeling. On the other hand, Mumford and Shah[8] introduced a functional for segmentation and smoothing of images modeled as piecewise continuous functions that are surrounded by discontinuities represented by contours. This functional was further approximated for implementation using various methods (e.g., see Refs. 2 and 9–15). A functional similar to the one proposed in Ref. 8, based on second variation was also investigated by Mahmoodi and Sharif for signal segmentation,[16,17] image segmentation, and noise reduction.[18] However it is well known that the optimal solution of nonlinear functionals considered in Ref. 8 is not unique,[12] which causes the implementing algorithms to fall into local minima. In this paper, a modification to the functional considered in Refs. 16–18 is proposed to enable the algorithm to segment and reconstruct structural texture images leading to an unsupervised texture segmentation method. Theoretically it is demonstrated in this paper that discontinuities are minimizers of the proposed functional, hence the second variation of the functional with respect to contour variations should generally be considered to discard contours that do not correspond to any discontinuity. It is conjectured that the proposed functional in this paper and also in Refs. 16–18 has a unique minimizer. The main contributions of this paper are (1) to impose an implicit smoothing in contrast with the explicit smoothing considered in the previous works in the literature (see, e.g., Refs. 8, 12, and 16–18) and (2) to detect discontinuities separating regions with different amplitude spectra as minimizers of the proposed functional. In comparison with texture segmentation algorithms with variational approaches, the method proposed in this paper is an unsupervised texture segmentation algorithm, while the texture segmentation method proposed in Ref. 4 is a supervised algorithm requiring a learning procedure. Furthermore, it is interesting to note that the proposed algorithm is also less expensive than methods based on feature space produced by Gabor filters.[3,5] This is so because the proposed variational algorithm is not required to generate any feature data from the original image prior to segmentation. On the other hand,

Paper 05192RR revised manuscript received Oct. 24, 2005 and Mar. 28, 2006; accepted for publication Apr. 17, 2006; published online Jul. 24, 2006.
1017-9909/2006/15(3)/033006/8/$22.00 © 2006 SPIE and IS&T.

the lack of an algorithm to choose and create the best set of filters used in the texture segmentation for a given textured image, is the main drawback of the methods discussed in Refs. 3 and 5. In comparison with Markov random field methods (e.g., Refs. 19–25), the algorithm proposed in this study demonstrates better results and has much less numerical complexity. Although structural textures are considered in this paper, the generalization of the proposed functional, in a statistical framework using level set method for segmentation, to stochastic textures is an interesting subject for future study.

2 Theory and Implementation Methods

An image $g(x,y)$ is considered to compose of regions (patterns) R_i with different amplitude spectra, which are separated by discontinuities that are represented by a contour. If we consider $f_i(x,y)$ as the smoothed continuous function of class $C^k, k \geq 2$, in $R_i - \Gamma_i$, then a functional of the smoothed image f and contour Γ is defined as

$$E(f,\Gamma) = \frac{1}{2}\sum_i \int_{R_i-\Gamma_i} \int [f_i(x,y) - g(x,y)]^2 S_i(x,y)\mathrm{d}x\mathrm{d}y, \quad (1)$$

where $S_i(x,y)$ is a windowed function representing an open connected set R_i contained within Γ_i in which $g(x,y)$ has no discontinuities. We can also define $S_i(x,y)$ as

$$S_i(x,y) = \begin{cases} 1 & x,y \in R_i \\ 0 & x,y \notin R_i, \end{cases}$$

and $\Gamma = \{\Gamma_i\}$. In computer vision terms, $S_i(x,y)$ is the segmented image, and $f_i(x,y)$ is the reconstructed image. In Refs. 8 and 16–18, a smoothing term is presented to guarantee that $f_i(x,y)$ is C^2 over R_i. However, in this paper we impose implicit smoothing by assuming that $f_i(x,y)$ can be written as a finite series of the linear combination of the C^∞ eigenfunctions such as sine and cosine functions, i.e.,

$$f_i(x,y) = \sum_m \sum_n [A_{imn}\cos(mux + nvy) + B_{imn}\sin(mux + nvy)]. \quad (2)$$

Equation (2) guarantees that $f_i(x,y)$ is smooth, since its composing eigenfunctions are C^∞. This restriction implies that $f_i(x,y)$ is continuous and differentiable in R_i. In fact, Eq. (2) represents the 2-D Fourier series of $f_i(x,y)$, and A_{imn} and B_{imn} are the Fourier coefficients. Our objective is to find $f_i(x,y)$ of C^k class ($k \geq 2$) and $S_i(x,y)$ that minimize the functional of Eq. (1). Let us assume that $f_i(x,y)$ satisfies the following equations:

$$f_i(-x,-y) = f_i(x,y),$$

$$f_i(x,-y) = f_i(-x,y).$$

The preceding assumptions decrease the number of required parameters by half, without any loss of generality, thus increasing the numerical efficiency of the algorithm and leading to half-range expansion of $f_i(x,y)$ where $B_{imn} = 0$ and A_{imn} is given as[26]

$$A_{imn} = \iint f_i(x,y)\cos(mux + nvy)\mathrm{d}x\mathrm{d}y,$$

Therefore the functional of Eq. (1) is rewritten as

$$E(\mathbf{A},\Gamma) = \frac{1}{2}\sum_i \int_{R_i-\Gamma_i} \int \left[\sum_m \sum_n A_{imn}\cos(mux + nvy) - g(x,y)\right]^2 S_i(x,y)\mathrm{d}x\mathrm{d}y, \quad (3)$$

where $\mathbf{A}$ can be considered as a matrix whose elements are A_{mn}.

The problem is now reduced to obtain the coefficients A_{imn} and $S_i(x,y)$ that minimize the functional of Eq. (3). To find an optimal solution for A_{ipq}, $S_i(x,y)$ is initially assumed fixed and the derivative of Eq. (3) with respect to A_{ipq} is set to zero, i.e.,

$$\frac{\partial E}{\partial A_{ipq}} = \int_{R_i-\Gamma_i} \int \cos(pux + qvy)\left[\sum_m \sum_n A_{imn}\cos(mux + nvy) - g(x,y)\right] S_i(x,y)\mathrm{d}x\mathrm{d}y = 0.$$

This then leads to the following linear system:

$$\sum_m \sum_n \int_{R_i-\Gamma_i} \int A_{imn}\cos(pux + qvy)\cos(mux + nvy)S_i(x,y)\mathrm{d}x\mathrm{d}y = \int_{R_i-\Gamma_i} \int g(x,y)\cos(pux + qvy)S_i(x,y)\mathrm{d}x\mathrm{d}y \quad \text{for } p,q \geq 0. \quad (4)$$

In this part, we aim to theoretically demonstrate that contours representing the discontinuities in functions $f_i(x,y)$ and hence coefficients A_{mn} over different regions are indeed minimizers of the functional of Eq. (3). Variations of the functional (1) can be calculated in a small neighborhood of an arbitrary point P on contour Γ_i between two regions S_i and S_{i+1}. If Γ_i is varied to Γ_i^+ and Γ_i^- in the neighborhood I of point P on the contour, the variations of the functional (1) are calculated as

$$E^+(f^+,\Gamma^+) = \frac{1}{2}\sum_i \int_{R_i^+-\Gamma_i^+} \int \{[f_i^+(x,y) - g(x,y)]^2\} S_i^+(x,y)\mathrm{d}x\mathrm{d}y,$$

$$E^-(f^-,\Gamma^-) = \frac{1}{2}\sum_i \int_{R_i^--\Gamma_i^-} \int \{[f_i^-(x,y) - g(x,y)]^2\} S_i^-(x,y)\mathrm{d}x\mathrm{d}y,$$

$$\delta E^{+} = E^{+} - E = \frac{1}{2}\sum_{j=i}^{i+} \int_{R_j^{+}-\Gamma_j^{+}} \int \{[f_j^{+}(x,y) - g(x,y)]^2\} S_j^{+}(x,y)\mathrm{d}x\mathrm{d}y - \frac{1}{2}\sum_{j=i}^{i+1} \int_{R_j-\Gamma_j} \int \{[f_j(x,y) - g(x,y)]^2\} S_j(x,y)\mathrm{d}x\mathrm{d}y,$$

and

$$\delta E^{-} = E - E^{-} = \frac{1}{2}\sum_{j=i}^{i+1} \int_{R_j-\Gamma_j} \int \{[f_j(x,y) - g(x,y)]^2\} S_j(x,y)\mathrm{d}x\mathrm{d}y - \frac{1}{2}\sum_{j=i}^{i+1} \int_{R_j^{-}-\Gamma_j^{-}} \int \{[f_j^{-}(x,y) - g(x,y)]^2\} S_j^{-}(x,y)\mathrm{d}x\mathrm{d}y.$$

The first variation with respect to contour variation can then be written as

$$\delta E = \delta E^{+} + \delta E^{-} = \frac{1}{2}\int_I \int \{[f^{+}(x,y) - g(x,y)]^2 - [f^{-}(x,y) - g(x,y)]^2\}\mathrm{d}x\mathrm{d}y, \tag{5}$$

where f^{+} and f^{-} are defined as

$$f^{+} = \begin{cases} f_i^{+} = \sum_m \sum_n A_{imn}^{+} \cos(mux + nvy) & (x,y) \in I \,\&\, (x,y) \in R_i \\ f_{i+1}^{+} = \sum_m \sum_n A_{(i+1)mn}^{+} \cos(mux + nvy) & (x,y) \in I \,\&\, (x,y) \in R_{i+1} \\ \text{unchanged} & (x,y) \notin I. \end{cases}$$

$$f^{-} = \begin{cases} f_i^{-} = \sum_m \sum_n A_{imn}^{-} \cos(mux + nvy) & (x,y) \in I \,\&\, (x,y) \in R_i \\ f_{i+1}^{-} = \sum_m \sum_n A_{(i+1)mn}^{-} \cos(mux + nvy) & (x,y) \in I \,\&\, (x,y) \in R_{i+1} \\ \text{unchanged} & (x,y) \notin I. \end{cases}$$

By using Eq. (5), in the neighbourhood I, the optimal contour corresponding to $\delta E=0$ (first minimization condition) can therefore be approximated as

$$[f^{+}(x,y) - g(x,y)]^2 - [f^{-}(x,y) - g(x,y)]^2 = 0.$$

By using δE^{+} and δE^{-} as already considered above, the second variation is calculated as

$$\delta^2 E^{-} = \delta E^{+} - \delta E^{-} = \frac{1}{2}\int_I \int \{[f^{+}(x,y) - g(x,y)]^2 - [f(x,y) - g(x,y)]^2\}\mathrm{d}x\mathrm{d}y + \frac{1}{2}\int_I \int \{[f^{-}(x,y) - g(x,y)]^2 - [f(x,y) - g(x,y)]^2\}\mathrm{d}x\mathrm{d}y.$$

To demonstrate that the second variation is positive in discontinuities, let us consider a simple case where an image consists of an object and background containing a single constant spatial frequency whose amplitude in the object is different from that in the background. This notion can then be generalized to objects and background with different spatial frequencies. Let us assume that the image inside the object (R_{object}) and the background (R_{back}) can be described as

$$g(x,y) = b_0 \cos(mux + nvy) \quad \text{for } (x,y) \in R_{\text{object}},$$

$$g(x,y) = b_1 \cos(mux + nvy) \quad \text{for } (x,y) \in R_{\text{back}},$$

where $b_0 \neq b_1$. If we also assume that the contour Γ surrounds the region R_{object}, then the linear system of Eq. (4) leads to $A_i=b_0$ and $A_o=b_1$. If Γ is varied to Γ^{+} so that R_{object}^{+} includes one part of the region where the amplitude of the constant spatial frequency $(mux+nvy)$ is b_1, then A_i^{+} and A_o^{+} are calculated as

$$A_o^{+} = \frac{\int\int g\cos(mux + nvy)S_{\text{back}}^{+}(x,y)\mathrm{d}x\mathrm{d}y}{\int\int \cos^2(mux + nvy)S_{\text{back}}^{+}(x,y)\mathrm{d}x\mathrm{d}y} = \frac{b_1\int\int \cos^2(mux + nvy)S_{\text{back}}^{+}(x,y)\mathrm{d}x\mathrm{d}y}{\int\int \cos^2(mux + nvy)S_{\text{back}}^{+}(x,y)\mathrm{d}x\mathrm{d}y} = b_1,$$

$$A_i^{+} = \frac{\int\int g\cos(mux + nvy)S_{\text{object}}^{+}(x,y)\mathrm{d}x\mathrm{d}y}{\int\int \cos^2(mux + nvy)S_{\text{object}}^{+}(x,y)\mathrm{d}x\mathrm{d}y},$$

$$A_i^{+} = \frac{\int\int g\cos(mux + nvy)S_{\text{object}}(x,y)\mathrm{d}x\mathrm{d}y + \int\int g\cos(mux + nvy)[S_{\text{object}}^{+}(x,y) - S_{\text{object}}(x,y)]\mathrm{d}x\mathrm{d}y}{\int\int \cos^2(mux + nvy)S_{\text{object}}(x,y)\mathrm{d}x\mathrm{d}y + \int\int \cos^2(mux + nvy)[S_{\text{object}}^{+}(x,y) - S_{\text{object}}(x,y)]\mathrm{d}x\mathrm{d}y},$$

or

$$A_i^+ = \frac{b_0 \int\int \cos^2(mux + nvy) S_{\text{object}}(x,y)\,dx\,dy + b_1 \int\int \cos^2(mux + nvy)[S^+_{\text{object}}(x,y) - S_{\text{object}}(x,y)]\,dx\,dy}{\int\int \cos^2(mux + nvy) S_{\text{object}}(x,y)\,dx\,dy + \int\int \cos^2(mux + nvy)[S^+_{\text{object}}(x,y) - S_{\text{object}}(x,y)]\,dx\,dy}.$$

Let us assume:

$$I_0 = \int\int \cos^2(mux + nvy) S_{\text{object}}(x,y)\,dx\,dy,$$

$$I_1 = \int\int \cos^2(mux + nvy)[S^+_{\text{object}}(x,y) - S_{\text{object}}(x,y)]\,dx\,dy,$$

then

$$A_i^+ = \frac{b_0 I_0 + b_1 I_1}{I_0 + I_1} = b_0 + \frac{(b_1 - b_0) I_1}{I_0 + I_1}.$$

Therefore,

$$\delta E^+ = \frac{1}{2} \int\int \left[\frac{(b_1 - b_0) I_1}{I_0 + I_1} \right]^2 \times \cos^2(mux + nvy) S^+_{\text{object}}(x,y)\,dx\,dy > 0.$$

Similarly, it can be shown that $\delta E^- < 0$. Hence $\delta^2 E = \delta E^+ - \delta E^- > 0$, i.e., the second variation is positive for Γ_i (second minimization condition). However, if Γ_i is away from any discontinuity, although the first minimization condition (i.e., $\delta E = 0$) is reached, the second condition is not satisfied (i.e., $\delta^2 E$ is not positive, in fact, $\delta^2 E = 0$ for such a contour). This implies that the contours away from any discontinuity are saddle points of functional (1) and hence are not the solutions of our minimization problem. Intuitively, the preceding mathematical description indicates that images containing structural textures can be approximated by a linear combination of a set of continuous eigenfunctions (Fourier basis functions) and discontinuities separating regions with different eigenfunctions (amplitude spectra), are the minimizers of the functional (1). The minimization of the functional (1) can lead to the segmentation of regions with certain amplitude spectra and hence the detection of discontinuities.

To find the most optimised contour(s), the level set approach proposed by Chan and Vese,[10,14] Vese and Chan,[12] Chan *et al.*,[13] and Vese[15] is applied, which aims to minimise the following functional:

$$F(A_{imn}, A_{omn}, \varphi) = \int_R \int [g(x,y) - \sum_m \sum_n A_{imn} \cos(mux + nvy)]^2 H[\varphi(x,y)]\,dx\,dy + \int_R \int [g(x,y) - \sum_m \sum_n A_{omn} \cos(mux + nvy)]^2 \{1 - H[\varphi(x,y)]\}\,dx\,dy, \quad (6)$$

where φ is a Lipschitz function whose zero level $[\varphi(x,y) = 0]$ represents the contour. In Eq. (6) $H(\cdot)$ represents the Heaviside function and, therefore, for $\varphi(x,y) > 0$, $H[\phi(x,y)]$ represents the region inside the contour, and hence, $1 - H[\phi(x,y)]$ corresponds to the region outside of the contour. The functional (6) is equivalent to the functional (3) in the level set framework. By using the same scheme as the one used to optimize the functional (3), the following linear system is obtained to find the most optimized coefficients A_{imn} for the region inside the contour

$$\int_R \int \cos(pux + qvy) g(x,y) H[\varphi(x,y)]\,dx\,dy = \sum_m \sum_n A_{imn} \int_R \int \cos(pux + qvy) \cos(mux + nvy) H[\varphi(x,y)]\,dx\,dy \quad p,q \geq 0. \quad (7)$$

The linear system of Eq. (7) is equivalent to Eq. (4) in the level set framework. A similar linear system can be obtained for coefficients A_{omn} for the region outside of the contour. The functional (6) is also minimized with respect to the signed distance function $\varphi(x,y)$, which then leads to the following Euler-Lagrange equation:[10]

$$\frac{\partial \varphi}{\partial t} = \delta_d(\varphi) \left\{ - \left[g - \sum_m \sum_n A_{imn} \cos(mux + nvy) \right]^2 + \left[g - \sum_m \sum_n A_{omn} \cos(mux + nvy) \right]^2 \right\}, \quad (8)$$

where $\delta_d(\varphi)$ is the derivative of Heaviside function, known as the Dirac function. The differential Eq. (8) coupled with a linear system such as Eq. (7) for the regions inside and outside of contour should be solved iteratively. The contour is iteratively evolved to converge to the desired solution, and on convergence, the contour corresponding to the zero level of φ $[\varphi(x,y) = 0]$ then represents the optimized contour. Fourier coefficients A_{imn} and A_{omn} for the regions inside and outside the contour, are used to reconstruct the image. Regularization of the Direc delta and Heavside functions used in differential Eq. (8) are performed as proposed in Ref. 10. An image may contain an indefinite number of frequency components whose coefficients are A_{imn}. In practice, it is intractable to calculate indefinite coefficients in a linear system such as Eq. (7). In fact, if the number of components involved in Eq. (7) increases, the algorithm becomes numerically expensive. To avoid this problem, in practice we search for frequency coefficients

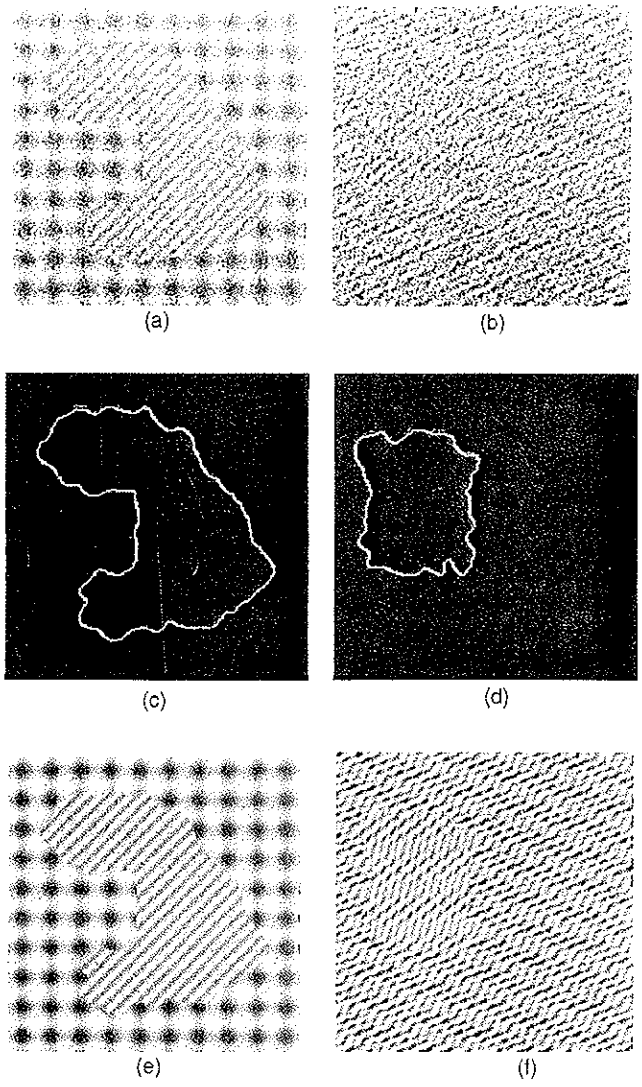

Fig. 1 Two synthetic textured noisy images with SNR=8.8 (a) and with SNR=3.3 (b), segmented (c) and (d) and reconstructed (e) and (f) images using the method proposed in this paper.

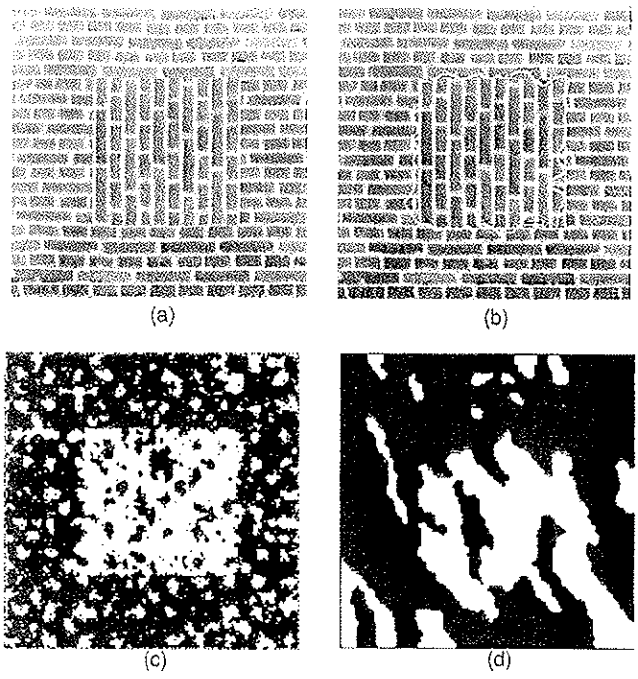

Fig. 2 Textured wall image (a) the detected contour representing the segmented textured objects using the method proposed in this paper (filter bandwidth= $\pi/7$) (b) the segmentation result based on the GMRF model using the AS-EM algorithm with second-order neighborhood with single resolution (c) and multi-resolution schemes (d).

that have significant powers and ignore the remaining coefficients. The amplitude spectrum of the image is used to find the most important frequency coefficients by examining the Fourier transform for inside and outside regions in each iteration. An adaptive thresholding scheme is employed in this algorithm as described in the pseudo-code at the end of this section. Differential Eq. (8) is then solved to update $\varphi(x,y)$ and hence the contour. Note that, in each iteration, a 2-D Gaussian filter is applied to $\varphi(x,y)$ to regularize partial differential Eq. (8), which improves the robustness of the proposed algorithm for textures characterized with sharp edges and also in noisy environments. The second variation of the functional with respect to zero level of φ does not need to be examined in the preceding level set framework. This is due to two reasons: (1) the number of regions (textures) to be segmented is known *a priori* and hence the necessary number of contours corresponding to the number of regions employed for segmentation is known; and (2) the first variation of the functional with respect to the contour variation, given in Eq. (8), therefore becomes zero in discontinuities and nonzero elsewhere, since the algorithm searches for contours separating regions different amplitude spectra. This prior knowledge enables the algorithm to rely on the first variation for segmentation. If two preceding assumptions are not made, then the second variation of the functional with respect to zero level set of φ must be examined to discard contours that do not correspond to any discontinuity. In summary, the implementation starts by choosing[10] the signed distance function as an initial function for φ, and the zero level of $\varphi\,[\varphi(x,y)=0]$ is the evolving curve. In each iteration, the Fourier transforms inside and outside of the contour are calculated and frequencies whose amplitudes are greater than the threshold are selected. The linear system of Eq. (7) for inside and outside of the contour is then solved to obtain the coefficients of frequency components. Finally, differential Eq. (8) is solved to update φ and hence to evolve the contour. Note that finite difference is used to solve differential Eq. (8). The algorithm converges when there is no significance change in the updated φ. In Eq. (8), we set Δt (steps in iteration) to unity. The initial value for the threshold should be set according to amplitudes of the most dominant frequency components of the textures. For instance, if the dominant frequency components are characterized with a low amplitude spectrum, a low initial value for the threshold must be set. This enables the algorithm to select the necessary frequency components. However, a higher value for the threshold is preferable for textures with strong dominant frequency components to avoid high numerical costs. The proposed algorithm written in pseudo-code is shown next.

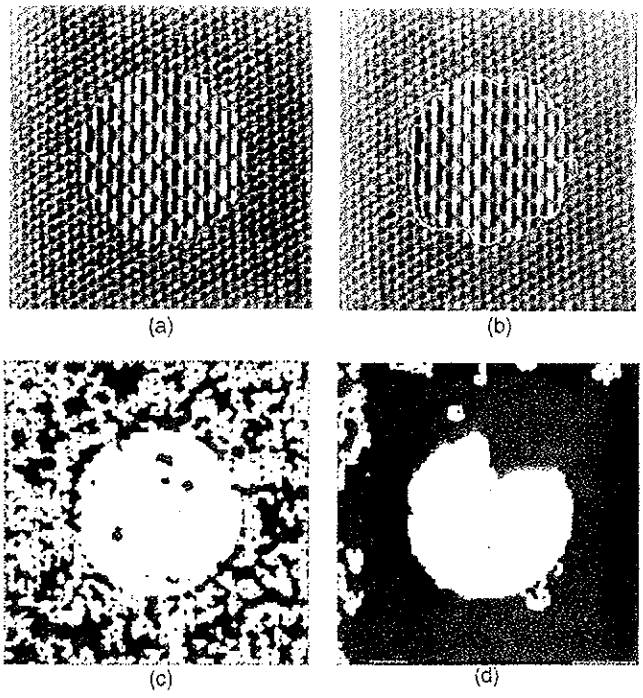

Fig. 3 Textured image consisting of the textures of Brodatz album (a) the detected contour separating two textures using the method proposed in this paper (filter bandwidth=$\pi/7$) (b) the segmentation result using the GMRF model based on the SA-EM algorithm with single resolution (c) and multiresolution schemes (d).

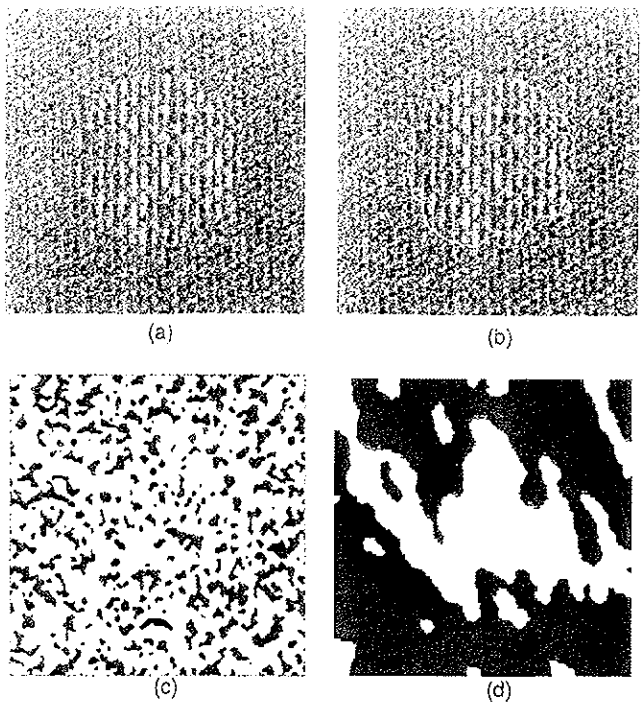

Fig. 4 Gaussian noise is added to the texture image of Fig. 3(a) to produce the noisy image of Fig. 4(a) with SNR=1.7 (a) the detected contour using the proposed algorithm in this paper (filter bandwidth=$\pi/10$) (b) the segmented image using the GMRF-based algorithm under single (c) and multiresolution schemes (d).

1. Initialize φ^0 and set an initial threshold T^0 for $n=0$

Loop:

2. Calculate the fast Fourier transform (FFT) of inside and outside regions of the contour and select frequencies whose amplitudes are greater than T^n

3. Compute A_{imn} and A_{omn} using the linear system (7)

4. Solve differential equation (8) *for φ to obtain φ^{n+1}*

5. Apply Gaussian low pass filter to φ^{n+1}

6. Discard the frequencies whose coefficients calculated in step 2, are not significant (i.e., they are less than 10% of the maximum coefficient)

***If** there are some discarded frequency components, **Then** update T^{n+1} by increasing its value; **Otherwise** decrease it*

***If** convergence is not reached, **Then** $n=n+1$ and go to step 2; **Otherwise** end the **Loop** and go to step 7*

7. Reconstruct the image using A_{imn} and A_{omn}

The threshold used in the preceding algorithm determines the number of frequency components that the algorithm detects for segmentation, i.e., the algorithm considers the frequency components whose amplitude is more than the threshold. An adaptive thresholding scheme is therefore considered in the proposed algorithm to iteratively change the threshold value to ensure that the number of detected frequency components is within a user-defined range governed by detection performance and computational costs.

3 Results

Two synthetic noisy images with SNR=8.8 and 3.3 are shown in Figs. 1(a) and 1(b). The algorithm described in Sec. 2 is applied to the noisy images of Fig. 1. The segmented and reconstructed images are shown in Figs. 1(c)–1(f).

To assess the performance of the proposed algorithm for real-world texture images, the examples shown in Figs. 2(a), 3(a), and 4(a) are considered. The segmented image achieved by applying the proposed algorithm to Fig. 2(a) is depicted in Fig. 2(b), and for the Gaussian Markov random field (GMRF) model in Fig. 2(c) and 2(d). In this case, the GMRF model with a second-order neighborhood for textures known as the autonormal model (e.g., see Refs. 19–22, 24, 25, and 27–29) is used. Simulated annealing (SA) is implemented based on the Gibbs sampler[30] with single and multiresolution schemes (for multiresolution schemes, e.g., see Refs. 22, 23, and 29). The parameter estimation for the GMRF model is obtained by using the expectation maximization (EM) procedure.[31] The image of Fig. 3(a) consists of two textures selected from the Brodatz album. Figure 3(b) shows the detected contour separating the two textures by applying the proposed method in Sec. 2. In Figs. 3(c) and 3(d), the segmented images are obtained by applying GMRF model to the image of Fig. 3(a). It is clear from Figs. 2 and 3 that the method proposed in this paper demonstrates a better performance. A quantitative comparison is provided in Table 1 at the end of this section for this example. The image of Fig. 3(a) is further contaminated with Gaussian noise to produce the noisy image of Fig. 4(a) with SNR=1.7.

Although multiresolution GMRF shows some improvement with respect to single-resolution GMRF, as demonstrated in Fig. 4(d), a better performance is observed by the

Table 1 A quantitative comparison in the segmentation error of the image of Fig. 3(a) for different algorithms considered in this paper.

Algorithms	Proposed Method	GMRF-SA-EM Single Resolution	GMRF-SA-EM Multiresolution
Error per pixel (%)	2.92	41.9	9.47

algorithm proposed in this paper. The detected contour achieved by applying the proposed level set method is shown in Fig. 4(b), whereas the GMRF-based model using the single-resolution scheme fails to segment the image in this noisy environment as depicted in Fig. 4(c). In structural textures such as those shown in Figs. 2 and 3, which are characterized with sharp edges, the number of frequency components composing the texture is numerically intractable for the texture reconstruction, however, segmentation is performed based on the frequency components with significant amplitudes. For instance, 11 frequency components are used by the algorithm for the segmentation of the image shown in Fig. 3. The algorithm proposed in this paper is also numerically more efficient than the GMRF-based segmentation algorithm. On a PC workstation with a 2.5 GHz CPU clock, for the segmentation of the image shown in Fig. 3, it takes 312 CPU seconds (22 iterations) for the level-set-based algorithm to converge, while the convergence of the SA-GMRF model requires 3000 iterations (each iteration around 45 s). It is well known that simulated annealing is a very expensive algorithm with logarithmic scheduling.[30] Note also that the GMRF-based algorithm can account for properties considered in a small neighborhood of each site due to Markovian properties. Therefore, the observed properties in neighborhoods with larger scales such as the images shown in Figs. 2 and 3 cannot be detected in such a framework. However, this problem is not present in the proposed algorithm. It is also straightforward to generalize the level-set-method-based algorithm discussed in this paper for images with more than two textures (regions) using a multiphase level set framework proposed in Ref. 12 The segmentation results using GMRF-based algorithms and the proposed algorithm for the image of Fig. 3 are shown in a binary format in Fig. 5. For a quantitative comparison, the absolute differences between the segmentation target shown in Fig. 5(a) and the segmented images using different algorithms are calculated. This absolute difference representing an error term in segmentation is then normalised by the number of pixels in the original image to demonstrate the error per pixel. Table 1 shows the error per pixel in percent for the algorithms applied to the image of Fig. 3(a).

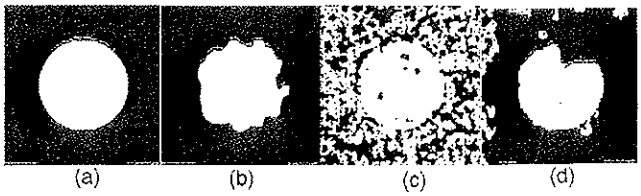

Fig. 5 Segmentation target for the image of Fig. 3 (a) the segmented image using the proposed algorithm in this paper in a binary format (b) the segmented images based on the GMRF model using the SA-EM algorithm under (c) single and (d) multiresolution schemes.

4 Conclusion

A functional based on implicit smoothing was considered in this paper for segmentation of structural textures, and equations minimizing this functional were also derived. It was demonstrated that the contours representing discontinuities in amplitude spectrum between two different patterns (regions) are the minimizers of the functional. The coefficients of the frequency components composing the texture can therefore be determined by minimizing the functional with respect to the coefficients. A reconstructed image can finally be generated using these coefficients. The level set method was used for implementation purposes. A comparison with a GMRF-based algorithm demonstrates a better performance for the algorithm proposed in this paper. The proposed level-set-based algorithm is also robust in the presence of noise. The generalization of the proposed functional in a statistical framework for segmentation of statistical textures is an interesting subject for future research.

References

1. M. Kass, A. Witkin, and D. Terzopoulos, "Snakes: Active contour models," *Int. J. Comput. Vis.* **1**, 321–331 (1987).
2. G. Aubert and P. Kornprobst, *Mathematical Problems in Image Processing: Partial Differential Equations and Calculus of Variations*, Springer-Verlag, New York (2002).
3. C. Sagiv, N. A. Sochen, and Y. Zeevi, "Texture segmentation via a diffusion-segmentation scheme in the Gabor feature space," in *Proc. Texture 2002, 2nd Int. Workshop on Texture Analysis and Synthesis* (June 2002).
4. N. Paragios and R. Deriche, "Geodesic active regions and level set methods for supervised texture segmentation," *Int. J. Comput. Vis.* **46**(3), 223–247 (2002).
5. T. Brox, M. Rousson, R. Deriche, and J. Weickert, "Unsupervised segmentation incorporating colour, texture and motion," in *Computer Analysis of Images and Patterns*, Lecture Notes in Computer Science Vol. 2756, pp. 353–360, Springer, Berlin (2003).
6. L. A. Vese and S. J. Osher, "Modelling textures with the total variation minimisation and oscillating patterns in image processing," *J. Sci. Comput.* **19**(1–3), 553-572 (2003).
7. L. I. Rudin, S. Osher, and E. Fatemi, "Nonlinear total variation based noise removal algorithms," *Physica D* **60**, 259–268 (1992).
8. D. Mumford and J. Shah, "Optimal approximations by piecewise smooth functions and associated variational problems," *Commun. Pure Appl. Math.* **42**(4), 577–688 (1989).
9. A. Tsai, A. Yezzi, and A. S. Willsky, "Curve evolution implementation of the Mumford-Shah functional for image segmentation, denoising, interpolation and magnification," *IEEE Trans. Image Process.* **10**(8), 1169–1186 (2001).
10. T. F. Chan and L. A. Vese, "Active contours without edges," *IEEE Trans. Image Process.* **10**(2), 266–277 (2001).
11. M. Hintermuller and W. Ring, "An inexact-CG-type active contour approach for the minimization of the Mumford-Shah functional," *J. Math. Imaging Vision* **20**, 19–42 (2004).
12. L. A. Vese and T. F. Chan, "A multiphase level set framework for image segmentation using the Mumford and Shah model," *Int. J. Comput. Vis.* **50**(3), 271–293 (2002).
13. T. F. Chan, B. Y. Sandberg, and L. A. Vese, "Active contours without edges for vector-valued images," *J. Visual Commun. Image Represent* **11**, 130–141 (2000).
14. T. F. Chan and L. A. Vese, "Level set algorithm for minimising the Mumford-Shah functional in image processing," in *Proc. IEEE Workshop on Variational and Level Set Methods in Computer Vision*, pp. 161–168 (2001).
15. L. A. Vese, "Multiphase object detection and image segmentation," in *Geometrical Level Set Methods in Imaging, Vision, and Graphics*, S. Osher and N. Paragios, Eds., pp. 175–194, Springer Verlag, New York (2003).
16. S. Mahmoodi and B. S. Sharif, "Signal segmentation and denoising algorithm based on energy optimisation," *Signal Process.* **85**(9), 1845–1851 (2005).

17. S. Mahmoodi and B. S. Sharif, "Noise reduction, smoothing, and time interval segmentation of noisy signals using an energy optimisation method," *IEE Proc. Vision Image Signal Process.* **153**(2), 101–108 (2006).
18. S. Mahmoodi and B. S. Sharif, "Nonlinear optimisation method for image segmentation and noise reduction using geometrical intrinsic properties," *Image Vis. Comput.* **24**, 202–209 (2006).
19. B. S. Manjunath and R. Chellapa, "Unsupervised texture segmentation using Markov random field models," *IEEE Trans. Pattern Anal. Mach. Intell.* 13(5), 478–482 (1991).
20. R. Chellapa, "Two dimensional discrete Gaussian Markov random models for image processing," in *Progress in Pattern Recognition 2*, L. N. Kanal and A. Rosenfeld, Eds. (1985).
21. B. S. Manjunath, T. Simchony, and R. Chellapa, "Stochastic and deterministic networks for texture segmentation," *IEEE Trans. Acoust., Speech, Signal Process.* **38**(6), 1039-1049 (1990).
22. S. Krishnamachari and R. Chellapa, "Multi-resolution Gauss-Markov random field models for texture segmentation," *IEEE Trans. Image Process.* **6**(2), 251–267 (1997).
23. R. Wilson and C. T. Li, "A class of discrete multi-resolution random fields and its application to image segmentation," *IEEE Trans. Pattern Anal. Mach. Intell.* **25**(1), 42–56 (2002).
24. S. Stan, G. Palubinskas, and M. Datcu, "Bayesian selection of the neighbourhood order for Gauss Markov texture models," *Pattern Recogn. Lett.* **23**, 1229–1238 (2002).
25. W. Pieczynski and A. N. Tebbache, "Pair-wise Markov random fields and segmentation of textured images," *Mach. Graphics Vision* **9**(4), 705–718 (2000).
26. E. Kreyszig, *Advanced Engineering Mathematics*, Wiley, New York (1999).
27. G. Winkler, *Image Analysis, Random Fields and Dynamic Monte Carlo Methods*, Springer-Verlag, Berlin (1995).
28. G. L. Gimel'farb, *Image Textures and Gibbs Random Fields*, Kluwer Academic, Boston (1999).
29. M. L. Comer and E. J. Delp, "Segmentation of textured images using a multi-resolution Gaussian autoregressive model," *IEEE Trans. Image Process.* 8(3), 408-420 (1999).
30. S. Geman and D. Geman, "Stochastic relaxation, Gibbs distributions and the Bayesian restoration of images," *IEEE Trans. Pattern Anal. Mach. Intell.* 6(6), 721-741 (1984).
31. A. P. Dempster, N. M. Laird, and D. B. Rubin, "Maximum likelihood from incomplete data via the EM algorithm," *J. R. Stat. Soc. Ser. B. Methodol.* **1**, 1–38 (1977).
32. S. C. Zhu, Y. Wu, and D. Mumford, "Filters, random fields and maximum entropy (FRAME): towards a unified theory for texture modelling," *Int. J. Comput. Vis.* **27**(2), 107–126 (1998).

Biographies and photographs of authors not available.